

AD-A043 545

ENVIRONMENTAL RESEARCH INST OF MICHIGAN ANN ARBOR IN--ETC F/6 15/4
STATISTICAL ANALYSIS OF TERRAIN BACKGROUNDS.(U)
AUG 77 J R MAXWELL

N00123-77-C-0682

UNCLASSIFIED

FRIM-129A00-1-T

AM

| OF |
AD
A043 545



END
DATE
FILMED
9-77
DDC

ADA 043545

g

12

Technical Report

STATISTICAL ANALYSIS OF TERRAIN BACKGROUND

Infrared and Optics Division

AUGUST 1977

Approved for Public Release;
Distribution Unlimited

Optical Signatures Program
Naval Weapons Center
China Lake, California

DDC
RECEIVED
AUG 30 1977
RECEIVED
RE B

HJ NO.
DDC FILE COPY

ENVIRONMENTAL
RESEARCH INSTITUTE OF MICHIGAN
FORMERLY WILLOW RUN LABORATORIES, THE UNIVERSITY OF MICHIGAN
BOX 618 • ANN ARBOR • MICHIGAN 48107

Unclassified

SECURITY CLASSIFICATION OF THIS PAGE (When Data Entered)

12

REPORT DOCUMENTATION PAGE		READ INSTRUCTIONS BEFORE COMPLETING FORM
1. REPORT NUMBER 129800-1-T	2. GOVT ACCESSION NO.	3. RECIPIENT'S CATALOG NUMBER
4. TITLE (and Subtitle) 6 Statistical Analysis of Terrain Backgrounds.		5. TYPE OF REPORT & PERIOD COVERED 9 Technical rept.
7. AUTHOR(s) 10 J. R. Maxwell		6. PERFORMING ORG. REPORT NUMBER 14 ERIM-129800-1-T
9. PERFORMING ORGANIZATION NAME AND ADDRESS Environmental Research Institute of Michigan Infrared and Optics Division P O Box 8618, Ann Arbor, MI 48107		8. CONTRACT OR GRANT NUMBER(s) 15 N00123-77-C-0682
11. CONTROLLING OFFICE NAME AND ADDRESS Dr. Lowell Wilkins, Code 39403 Naval Weapons Center China Lake, CA 93555		10. PROGRAM ELEMENT, PROJECT, TASK AREA & WORK UNIT NUMBERS Task SH 3773 292344 Program Element 62332N Project ZF32-392-002
14. MONITORING AGENCY NAME & ADDRESS (if different from Controlling Office)		12. REPORT DATE 11 August 1977
		13. NUMBER OF PAGES 12 34 p.
		15. SECURITY CLASS. (of this report) Unclassified
16. DISTRIBUTION STATEMENT (of this Report) 16 F32392, SH3773 Approved for public release; distribution unlimited.		15a. DECLASSIFICATION/DOWNGRADING SCHEDULE
17. DISTRIBUTION STATEMENT (of the abstract entered in Block 20, if different from Report) Approved for public release; distribution unlimited.		DDC DECLASSIFIED AUG 30 1977 RESERVED B
18. SUPPLEMENTARY NOTES		
19. KEY WORDS (Continue on reverse side if necessary and identify by block number) Terrain backgrounds data, statistical analysis, multispectral data		
20. ABSTRACT (Continue on reverse side if necessary and identify by block number) High spatial resolution calibrated airborne multispectral scanner imagery of 7 terrain backgrounds have been analyzed statistically. The objective of analysis is to develop a methodology for characterizing various background types with parameters that can be used reliably in estimating sensor performance capabilities, especially false alarm rates. Imagery in several reflective IR spectral bands (1.0-1.4, 1.5-1.8, and 2.0-2.6 m) & thermal IR bands (4.5-5.5 & 9.3-11.7 m) have been analyzed for residential, industrial, mountainous, forested and desert terrain. kilometers		

DD FORM 1473 1 JAN 73

EDITION OF 1 NOV 65 IS OBSOLETE
S/N 0102-014-6601

UNCLASSIFIED

SECURITY CLASSIFICATION OF THIS PAGE (When Data Entered)

408259

UNCLASSIFIED

SECURITY CLASSIFICATION OF THIS PAGE (When Data Entered)

~~Results~~. Results of a conventional statistical analysis of mean apparent radiances/temperatures, standard deviations, probability density functions, spectral correlations, and one and two dimensional Wiener spectra are presented. The Wiener spectrum is a useful statistic for estimating the average system noise generated by background clutter. However it is well known that when the probability density function is non-Gaussian, the Wiener spectrum analysis is generally not useful for estimating the occurrence of rare events and that it generally provides erroneous false alarm rate estimates. None the less, the Wiener spectrum analysis is elegant and is often the only means of analysis available because of a lack of data, suitable statistics, and/or a more appropriate methodology.

The statistical results that are shown demonstrate that terrain backgrounds are indeed non-Gaussian. A new methodology has been developed and is presented which is a logical extension of the familiar pulse height, pulse length, and threshold exceedence statistics used to characterize one-dimensional signals. For each of several intensity threshold settings in the two dimensional scene data, contiguous areas which exceed the threshold are identified. An ellipse for each contiguous area at each intensity threshold level is then defined with the same area, second moment, and orientation. The numbers, sizes, shapes, and orientations of elliptical areas at each threshold are then the parameters used to describe the spatial characteristics of the scene. These area/intensity statistics clearly include in their characterization the frequency of occurrence of small high intensity areas which cause false alarms vs small lower intensity areas which do not (a distinction that cannot be made on the basis of a Wiener spectra characterization).

Results of area/intensity scene analysis are presented and current simulation efforts to analyze sensor false alarm rates using actual backgrounds data and backgrounds data generated by equivalent ellipses are discussed.

UNCLASSIFIED

SECURITY CLASSIFICATION OF THIS PAGE (When Data Entered)

TABLE OF CONTENTS

LIST OF FIGURES 4

LIST OF TABLES 5

1. INTRODUCTION 6

2. CONVENTIONAL STATISTICS 7

 2.1 Means, Standard Deviations, and Histograms 7

 2.2 Spectral Correlations 9

 2.3 Wiener Spectra 9

3. AREA/INTENSITY STATISTICS 10

4. CURRENT EFFORTS 11

5. SUMMARY 12

REFERENCES 34

ACCESSION for	
NTIS	White Section <input checked="" type="checkbox"/>
DDC	Buff Section <input type="checkbox"/>
UNANNOUNCED	<input type="checkbox"/>
JUSTIFICATION _____	
BY _____	
DISTRIBUTION/AVAILABILITY CODES	
Dist	1 / OF SPECIAL
A	

LIST OF FIGURES

1.	HISTOGRAM OF SIX AREAS WITHIN THE RESIDENTIAL FLINT-1 AREA IN THE 9.3 - 11.7 μm SPECTRAL BAND	20
2.	HISTOGRAM OF RESIDENTIAL FLINT-1 AREA	21
3.	HISTOGRAM OF INDUSTRIAL FLINT-2 AREA	22
4.	HISTOGRAM OF WICHITA MOUNTAINS, OKLAHOMA, MILL CREEK FLIGHT MISSION	23
5.	HISTOGRAM OF BALTIMORE AREA	24
6.	HISTOGRAM OF BLACK HILLS-1 AREA	25
7.	HISTOGRAM OF BLACK HILLS-2 AREA	26
8.	HISTOGRAM OF MONO LAKE AREA	27
9.	HISTOGRAM OF PISGAH CRATER AREA	28
10.	AVERAGE OF WIENER SPECTRUM OF EACH SCAN LINE IN FLINT-1 IMAGE	29
11.	AVERAGE OF WIENER SPECTRUM OF A PORTION OF EACH SCAN LINE LOOKING AT UNIFORM DARK LEVEL WITHIN SCANNER HOUSING IN FLINT-1 IMAGE	29
12.	AVERAGE OF WIENER SPECTRUM OF EACH SCAN LINE IN WICHITA MOUNTAINS OF OKLAHOMA, DATA OF MILL CREEK MISSION	30
13.	EQUIVALENT ELLIPTICAL AREAS FOR CONTIGUOUS AREA IN THE FLINT-1 IMAGE WITH APPARENT TEMPERATURES GREATER THAN 303.8 K OR 3σ ABOVE THE MEAN	31
14.	EQUIVALENT ELLIPTICAL AREAS FOR CONTIGUOUS AREAS IN THE FLINT-1 IMAGE WITH APPARENT TEMPERATURE GREATER THAN 299.1 K OR 1.5σ ABOVE THE MEAN SUPERIMPOSED ON THE ACTUAL FLINT-1 9.3 - 11.7 μm IR IMAGE	32
15.	ACTUAL IMAGE OF FLINT-1 (LEFT) AND AN ELLIPSE REPRESENTATION OF FLINT-1 IMAGE (RIGHT)	33

LIST OF TABLES

I.	MULTISPECTRAL DATA PARAMETER SUMMARY	13
II.	CORRELATION MATRIX, RESIDENTIAL FLINT-1	14
III.	CORRELATION MATRIX, RESIDENTIAL FLINT-2	14
IV.	CORRELATION MATRIX, WICHITA MOUNTAINS, OKLAHOMA, MILL CREEK MISSION	14
V.	CORRELATION MATRIX, BALTIMORE.	15
VI.	CORRELATION MATRIX, BLACK HILLS-1	15
VII.	CORRELATION MATRIX, BLACK HILLS-2	15
VIII.	CORRELATION MATRIX, MONO LAKE.	15
IX.	CORRELATION MATRIX, PISGAH CRATER	16
X.	DISTRIBUTION OF ELLIPSES BY AREA AT 1.5, 2.0, 2.5, 3.0 σ THRESHOLDS FOR THE 9.3 - 11.7 μm FLINT-1 IMAGE.	16
XI.	DISTRIBUTION OF ELLIPSES BY AREA AT 1.5, 2.0, 2.5, 3.0 σ THRESHOLDS FOR THE 1.0 - 1.4 μm FLINT-1 IMAGE	17
XII.	DISTRIBUTION OF ELLIPSES BY AREA AT 1.5, 2.0, 2.5, 3.0 σ THRESHOLDS FOR THE 9.3 - 11.7 μm WICHITA MOUNTAINS IMAGE.	18
XIII.	DISTRIBUTION OF ELLIPSES BY AREA AT 1.5, 2.0, 2.5, 3.0 σ THRESHOLDS FOR THE 1.0 - 1.4 μm WICHITA MOUNTAINS IMAGE	19

1.0 INTRODUCTION*

One of the most difficult aspects of estimating a sensor's performance characteristics has to do with how well it will actually do in acquiring and tracking its target against the real world backgrounds. A wide variety of spatial and spectral processing techniques are used in today's sensor systems. These techniques are generally designed on the basis of specific and detailed knowledge of the signature characteristics of the targets, but with only limited information about the signature characteristics of the backgrounds. Design goals are often based on mean radiance levels and root mean square (rms) variations in the background clutter even though it is well known that it is often only the rarely occurring events, those not reflected in the rms level, that cause the false alarms.

The overall problem which this program is directed to is improving the capability of sensor systems to acquire and track targets and discriminate against the background clutter of the real world.

The specific objectives of this background analysis effort are: 1) to develop statistical descriptions of backgrounds that are appropriate for sensor systems analyses against real world backgrounds; and 2) to correlate these statistical parameters with generic backgrounds descriptions so that meaningful sensor systems specifications against different real world background types can be written.

A summary of available background measurement data was made at the outset of this program. About 230 documents have been annotated in an "Infrared Background Survey and Analysis Report" that is available through DDC [1]. Most of the existing data do not provide both spectral and high spatial resolution data needed for estimating the performance characteristics of today's tactical sensors, especially for false track and false alarm rates of seeker and threat warning receiver-type sensors.

A unique source of data that does provide spectral and high spatial resolution data is the ERIM collection of multispectral scanner data [2]. Over 20,000 flight line miles of data have been taken in the last 10 years in support of NASA's Earth Resources Program.

The ERIM multispectral scanner imagery are particularly well suited for analyzing the signatures of terrain backgrounds. First, the data are in the form of imagery. This provides spatial data in two dimensions. Second, the data in the various spectral bands extend from the ultraviolet (UV) into the thermal infrared (IR). Third, the data are collected simultaneously through a common optical aperture so that the spectral correlations between various pairs of spectral bands can be determined. Finally, the data are recorded on magnetic tape along with the necessary

* This work is sponsored by the Optical Signature Program, Naval Weapons Center, China Lake, CA, contract N00123-76-C-0708, under the direction of Lowell Wilkins. This paper was presented to the Twenty-Fifth National IRIS, 14 June 1977, in San Francisco, CA.

radiometric calibration signal levels so that the data are easily amenable to quantitative analyses.

The primary interest has been with data in the reflective IR from 1.0-1.4, 1.5-1.8, and 2.0-2.6 μm and in the thermal IR from 3-5 and 8-14 μm . The data selected for analyses were collected over residential areas of Flint and Baltimore, an industrial area of Flint, the Wichita mountains in Oklahoma (these data were collected along with primary mission data collected at Mill Creek, Oklahoma, hence the data have been labeled the Mill Creek data), a forested area in the Black Hills, and the desert type backgrounds near Pisgah Crater and Mono Lake in California. The data selected for processing were collected at aircraft altitudes of 1000-3000 feet. Imagery typically covers a ground area 2000 x 6000 feet with spatial resolutions of from 3-15 feet. The noise in the reflective IR channels varies with illumination level, and the noise in the thermal IR channels is a few tenths of a degree Kelvin. A summary of the data collection parameters is shown in Table I.

The data that were selected for analysis on this program were analog recorded. The standard processing techniques used with all of the data were to digitize the data, calibrate it, and format the data with one digital sample for each instantaneous field-of-view resolution element on the ground.

Multispectral scanner imagery for a variety of background types have been analyzed on this program. Conventional statistics have been determined for these scenes which include mean radiances in the reflective IR and mean apparent temperatures in the thermal IR, standard deviations, histograms, spectral correlations, and Wiener spectra. In addition, two-dimensional area/intensity statistics have also been developed for these scenes that are analogous to the familiar threshold crossing, pulse height, and pulse length statistics of one-dimensional signal analysis. Examples are presented in the following sections.

2.0 CONVENTIONAL STATISTICS

2.1 MEANS, STANDARD DEVIATIONS, AND HISTOGRAMS

Histograms for all of the multispectral scanner data analyzed in the reflective and thermal IR bands are shown in Figures 1-9. The log plots are shown to facilitate comparison with the Gaussian distribution having the same mean and standard deviation shown by the circled data points. The vertical scale is the probability density with respect to the bin number scale. The probability density with respect to the temperature or radiance scale can be obtained by multiplying the probability density with respect to the bin number scale by the factor $M = \Delta\text{Bin Number}/\Delta\text{temperature}$ or $\Delta\text{Bin Number}/\Delta\text{radiance}$. The horizontal scale is spectral radiance ($\mu\text{W}/\text{cm}^2\text{-sr}-\mu\text{m}$) for the reflective IR bands and apparent temperature (K) for the thermal IR bands. Apparent temperatures rather than radiances were chosen for the thermal IR data for the convenience of the user in converting to his own specific thermal IR spectral band.

A "Bin Number" scale is shown with each histogram so that the highest radiance or apparent temperature recorded without saturation can be identified. This occurs at the "Bin Number" of 255 and arises because of the eight-bit analog-to-

digital system used in converting the original data that was recorded on analog magnetic tape.

Occasionally the data on the original analog tape were saturated. This occurrence is identifiable by a large number of data points in the tail of the histogram at a bin number less than 255. Examples are the 9.3-11.7 μm Flint-1 data shown in Figure 2d, with the pile up of data points at about 308 K at the bin number of 220, and the 4.5-5.5 and 8.0-13.5 μm Black Hills-1 data in Figures 6c and 6d.

There are a great many differences in the histograms of data from the different background types in the reflective IR bands. Generally the mean values are low for the data collected early in the morning (Mill Creek, Figure 4). The histograms tend to vary widely, and especially noticeable are the large standard deviations and the very broad distributions in the Mill Creek data arising from the large ground shadows present in the early morning. In many of the data sets there are more data points with high radiance values than given by a Gaussian distribution.

There are a number of features that should be noted in the thermal IR data. Figure 1 shows histograms of the apparent temperatures in six areas of residential Flint-1 background data in the 9.3-11.7 μm spectral band. Clearly the scene is not homogeneous. Figure 2d shows a histogram of the entire residential area of Flint-1. The dynamic range of the data extends to almost four standard deviations above the mean before saturation. The main feature to be noticed in this data is the non-Gaussian character of the data, with an excess of data points with temperatures well above the mean.

Figure 4d, the Mill Creek data, shows a histogram of the 9.3-11.7 μm data collected over an area of the Wichita mountains in Oklahoma. These data were collected at 7:30 in the morning and the very tight distribution, with a standard deviation of less than 1 K, can be attributed to the "cross-over" phenomenon. As with the residential Flint-1 data shown in Figure 2d, there is an excess of occurrences beyond the 3σ point.

Figure 8c is the histogram for an area near Mono Lake, California in the 4.5-5.5 μm spectral band. The detailed types of features in the scene which cause the several peaks in this histogram have not been identified, but they are probably due to the sunlit and shadowed areas in the terrain which are differentially heated by the sun. Figure 8d is the histogram of the same Mono Lake area in the 8.0-13.5 μm spectral band. This histogram is nearly identical to the 4.5-5.5 μm histogram with one important difference: the mean apparent temperature is about 3 K higher. This suggests that the average terrain emittance is about 5% higher in the 8.0-13.5 μm spectral band.

Figure 9a is a histogram of an area of terrain near Pisgah Crater, California. These data are in the 8.0-10.9 μm spectral band and are pretty well described by a Gaussian distribution to two or three standard deviations above the mean. Figure 9b is a histogram of the same area taken in the 9.3-12.1 μm spectral band, and it is very much like that in the 8.0-10.9 μm spectral band. Figure 9c is another histogram of the same taken in the 11.3-13.5 μm spectral band. The significant difference is that these data were collected with a spatial resolution of 3.5 feet, whereas the data in Figures 9a and 9b were collected with a spatial resolution of

28 feet. The mean apparent temperatures are nearly the same, however the standard deviation is about 0.5 K larger so that there are proportionately many more scene elements at the higher temperatures in the high spatial resolution data.

2.2 SPECTRAL CORRELATIONS

Spectral correlations between the various spectral band pairs are shown in Tables II-IX. Correlations are only calculated when the data have been collected through a common aperture and are in spatial registration. Correlations have not been calculated between the 4.5-5.5 and 8.0-13.5 μm bands of the Black Hills-1 data because these data were not in exact registration. The Black Hills-1 and Black Hills-2 data were collected with two different scanners in the same aircraft so that their respective channels have not been correlated, and in fact the data from the two scanners may differ slightly because the scanner fields-of-view were somewhat different.

Table II shows spectral correlations between bands in the residential Flint-1 data. The correlations amongst the reflective IR bands are low, between 0.3 and 0.6, and this is probably due to the fact that there are many different materials in the scene, some with reflectances that increase with wavelength, others that do not. In general one would expect a rather low correlation between the reflective IR channels and the thermal IR channels although they sometimes are not small; for example, the 1.0-1.4 and 9.3-11.7 μm spectral correlation coefficient is -0.45.

Table IV shows the spectral correlations for the Wichita mountains, Oklahoma data obtained on the Mill Creek data collection mission. The spectral correlations are higher than they were for the residential Flint-1 area. Because these data were collected at 7:30 in the morning the high spectral correlations could be due to the presence of many large shadows or to a predominance of materials that tend to have a similar wavelength dependence to their reflectance.

Table IX shows the spectral correlation between the 8.0-10.9 μm and 9.4-12.1 μm spectral bands of the Pisgah Crater data. In view of the fact that they are adjacent spectral bands in the thermal IR and that the histograms (Figures 9a and 9b) are so similar, it might seem surprising that the correlation is only 0.7 to 0.8. However this particular data was collected to demonstrate the capability for discriminating various rock types on the basis of the reststrahlen band at 9.8 μm of some rock types. It may be the presence of the various rock types with their variable emittances at 9.8 μm that cause the lower than expected correlation coefficient.

2.3 WIENER SPECTRA

Wiener spectra have a long history in the IR community as a convenient way to describe the spatial characteristics of backgrounds. The literature is full of elegant linear systems analyses with powerful theory for determining various characteristics of the system output from the Wiener spectrum of the system's input. A frequent use of the Wiener spectrum is the rms of the output of a linear system from the Wiener spectrum of the input, and this is valid whether the input is Gaussian or not. The estimation of false track and false alarm

rates for many of today's seeker and threat warning sensors from the Wiener spectra of backgrounds, however, is much less reliable because of the non-Gaussian characteristics of so many backgrounds. The area/intensity statistics that have been developed on this program, and that will follow the discussion of the Wiener spectra of the data, may be more useful than the Wiener spectra for this application.

Figure 10 shows the Wiener spectra for the residential Flint-1 data in each of the four spectral bands of interest. Wiener spectra have been calculated for each scan line in the scene, and the average of the Wiener spectra for all of the lines in the image are averaged and shown in the figure. The ordinate on the Wiener spectrum plots is $(\mu\text{W}/\text{cm}^2 \text{-sr } \mu\text{m})^2/(\text{cy}/\text{m})$ for the 1-1.4, 1.5-1.8, and 2.0-2.6 μm bands, $(\text{K})^2/(\text{cy}/\text{m})$ for the 9.3-11.7 μm band. Two-dimensional Wiener spectra are included in Reference [3]. The lowest curve is the Wiener spectrum for the 9.3-11.7 μm band. At the lower spatial frequencies to about $10^{-1}/\text{m}$, the spatial frequency dependence is f^{-n} with n approximately 1. At high spatial frequencies n is 1.6. The Wiener spectra are similar for all spectral bands to about $10^{-1}/\text{m}$. The spatial frequency content at $10^{-1}/\text{m}$ in the thermal IR band might be from the houses that show so prominently in the residential Flint-1 thermal IR imagery. The spectrum of the multispectral scanner noise begins to dominate somewhat short of the spatial frequency limit of the detector as shown in Figure 11. The $5 \times 10^{-1}/\text{m}$ peak in the 1-1.4 μm data and the increase in the 2-2.6 μm data beyond $10^{-1}/\text{m}$ is due to noise in the system.

Figure 12 shows the Wiener spectra for the Wichita mountain, Oklahoma data. The spatial frequency content in the data is similar to that of the residential Flint-1 area data. The Wiener spectrum for the 9.3-11.7 μm band data has a f^{-n} dependence with $n = 1.15$ to $2 \times 10^{-2}/\text{m}$, and $n = 1.80$ to $10^{-1}/\text{m}$.

3.0 AREA/INTENSITY STATISTICS

Threshold crossing, pulse length, and pulse height statistics are more useful and reliable than Wiener spectra in analyzing the false track and false alarm characteristics of sensors that scan a detector in one dimension. The Wiener spectrum can be a very useful tool for estimating rms clutter levels at a sensor output, but the power spectrum does not distinguish between one scene that has a few small hot spots and another that has many not-so-hot spots. Yet the former is the scene that causes seekers and threat warning receivers false locks and false alarms. The latter is no trouble for today's sensors with any sophistication in the processing. A two-dimensional analog of these statistics is needed to analyze sensors that view large areas of background, for example the reticle seeker and the staring sensor, and the sensors that scan arrays of detectors and process in two dimensions, for example the mini-flir seekers and the threat warning receivers. The area/intensity statistics that have been developed on the current program is one approach to the needed two-dimensional analog.

The area/intensity statistics that have been developed on this program are best defined by the way they are generated. A threshold is set and each contiguous area above the threshold is identified. Then each contiguous area is replaced with an

elliptical area. The elliptical area is equivalent in that it has the same area and the same second moment as the contiguous area that it is representing. Ellipses are generated at each of several thresholds, and then the numbers of ellipses at each threshold are tabulated as a function of area, shape, and orientation.

The ellipses generated for the residential Flint-1 image in the 9.3-11.7 μm band with the threshold set at 303.8 K, three standard deviations above the mean apparent temperature for the scene, are shown in Figure 13. The equivalent ellipses that exceed a threshold set at 1.5σ above the mean, superimposed on the original 9.3-11.7 μm IR image collected over the residential Flint-1 area, are shown in Figure 14. It is clearly the roofs of the houses that are more than 4.7 K above the mean apparent temperature for the scene.

Table X shows histograms of the equivalent elliptical areas that exceed a threshold set at 1.5, 2.0, 2.5, and 3.0σ in the 9.3-11.7 μm band of the residential Flint-1 data. Table XII shows histograms of the ellipses in the 9.3-11.7 μm band of the Wichita mountains, Oklahoma data. These data show that there are relatively fewer hot spots in the residential Flint-1 data in the 9.3-11.7 μm band data.

4.0 CURRENT EFFORTS

The utility of the area/intensity statistics will depend in part on whether or not we will ultimately be able to infer something about them from a generic description of the background. We are currently examining the area/intensity ellipse statistics for other background types as well as extending our investigations to include cloud backgrounds as well as terrain backgrounds.

The utility of the area/intensity statistics will also depend on how much information the ellipses preserve of the spatial characteristics of the actual scene they represent. Clearly the ellipses do not preserve the spatial characteristics of sharp corners. On the other hand most sensors discriminate largely on areas, edges, and gradients. In addition, most sensor systems only process data over a limited portion of the scene. Hence, the ellipses may preserve all of the spatial information that is essential for determining how well a sensor will perform against a background of given "ellipse statistics".

In order to determine whether the spatial characteristics of the ellipses are adequate, we are currently using one of our actual background scenes in a reticle seeker simulation facility at China Lake. We are also using an ellipse representation of the background scene in the simulator, and we will compare results against the two scenes.

Figure 15 shows the actual image on the left and its ellipse representation on the right. We are not suggesting that in general the ellipse representation be used instead of the actual imagery in a simulator; rather it is currently being used in the simulation to validate the use of ellipses to describe the two-dimensional spatial characteristics of the background scenes. The actual image on the left is color-coded with areas in the scene with temperatures 1σ , 2σ , 3σ , and 4σ above the mean. This corresponds to the color coding of the 1σ , 2σ , 3σ , and 4σ

ellipses shown in the image on the right. The ellipses pretty clearly preserve a great deal of the spatial characteristics that are present in the original scene. Ellipse representations with the ellipses randomly positioned will be tested in the simulator to determine the degree to which higher order statistics are important.

5.0 SUMMARY

In summary, selected airborne multispectral scanner imagery have been calibrated and put into digital form, and a variety of conventional statistics have been reported.

We have generated area/intensity statistics in the form of histograms of ellipse areas at several thresholds.

We are now in the process of validating the utility of the ellipses, both as a statistic that might be related to generic descriptions of terrain and cloud backgrounds, and as a useful statistic for describing the two-dimensional spatial characteristics of backgrounds for false lock and false alarm rate analysis of today's sensor systems.

TABLE I. MULTISPECTRAL DATA PARAMETER SUMMARY

IMAGE	APPROXIMATE GROUND RESOLUTION (Ft.)	APPROXIMATE IMAGE SIZE (Ft.)	SPECTRAL BANDS (μm)
Flint-1 11:30 AM 18 Sep 71 Residential	2.5 x 5.0	1600 x 4000	1.0-1.4, 1.5-1.8, 2.0-2.6 9.3-11.7
Flint-2 11:55 AM 18 Sep 71 Urban	2.5 x 5.0	1600 x 4400	1.0-1.4, 1.5-1.8, 2.0-2.6 9.3-11.7
Baltimore 11:37AM 11 May 72 Residential	6.25 x 12.5	4000 x 5000	1.0-1.4, 2.0-2.6 9.3-11.7*
Mill Creek 7:33 AM 30 Jun 72 Mountains	7.5 x 15.0	4800 x 3900	1.0-1.4, 1.5-1.8, 2.0-2.6 9.3-11.7
Black Hills-1 (1) 1340 22 Jul 69 Forest	5.25 x 9.9	1100 x 7100	1.0-1.4, 2.0-2.6, 4.5-5.5, 8.0-13.5* 11.3-13.5*, 8.0-10.9, 9.4-12.1
Black Hills-2 1340 22 Jul 69 Forest	5.25 x 9.9	2400 x 7200	1.0-1.4, 1.5-1.8, 2.0-2.6 11.3-13.5*, 8.0-10.9, 9.4-12.1
Pisgah Crater 0822 AM 30 Oct 70 Desert	3.5 x 3.5 (2)	800 x 6800	11.3-13.5*, 8.0-10.9, 9.4-12.1
Mono Lake 0952 AM 23 Sep 68 Desert	26.0 x 26.0	3100 x 7500	1.0-1.4, 2.0-2.6, 4.5-5.5 8.0-13.5*

(1) Two different scanners were used on the same aircraft to collect the Black Hills-1 and Black Hills-2 data
 (2) The ground resolution for the laminar detector pair, 8.0-10.9 and 9.4-12.1, is 21 ft x 28 ft.
 * Data in this channel is not in exact spatial registration with data in other channels so that spectral correlations are not calculated

TABLE II. CORRELATION MATRIX, RESIDENTIAL FLINT-1

CORRELATION	1.0-1.4	1.5-1.8	2.0-2.6	9.3-11.7
1.0-1.4	1.000			
1.5-1.8	0.392	1.000		
2.0-2.6	0.303	0.603	1.000	
9.3-11.7	-0.455	0.048	0.177	1.000
CHANNELS	1.0-1.4	1.5-1.8	2.0-2.6	9.3-11.7
MEAN	1272	173	35.8	294.4
ST. DEVIATION	364	82.7	10.3	3.14

TABLE III. CORRELATION MATRIX, INDUSTRIAL FLINT-2

CORRELATION	1.0-1.4	1.5-1.8	2.0-2.6	9.3-11.7
1.0-1.4	1.000			
1.5-1.8	0.718	1.000		
2.0-2.6	0.489	0.634	1.000	
9.3-11.7	-0.437	-0.180	-0.036	1.000
CHANNELS	1.0-1.4	1.5-1.8	2.0-2.6	9.3-11.7
MEAN	789	239	39.2	297.0
ST. DEVIATION	305	77.8	13.7	3.17

TABLE IV. CORRELATION MATRIX, WICHITA MOUNTAINS, OKLAHOMA
MILL CREEK MISSION

CORRELATION	1.0-1.4	1.5-1.8	2.0-2.6	9.3-11.7
1.0-1.4	1.000			
1.5-1.8	0.835	1.000		
2.0-2.6	0.869	0.880	1.000	
9.3-11.7	0.052	0.256	0.245	1.000
CHANNELS	1.0-1.4	1.5-1.8	2.0-2.6	9.3-11.7
MEAN	112	35.9	4.17	298.1
ST. DEVIATION	62.2	20.1	2.91	.97

TABLE V. CORRELATION MATRIX, BALTIMORE

CORRELATION	1.0-1.4	2.0-2.6		
1.0-1.4	1.000			
2.0-2.6	0.084	1.000		
CHANNELS	1.0-1.4	2.0-2.6	9.3-11.7	
MEAN	2133	78.4	299.1	
ST. DEVIATION	777	43.8	5.88	

TABLE VI. CORRELATION MATRIX, BLACK HILLS-1

CORRELATION	1.0-1.4	2.0-2.6	4.5-5.5	
1.0-1.4	1.000			
2.0-2.6	0.505	1.000		
4.5-5.5	-0.166	0.498	1.000	
CHANNELS	1.0-1.4	2.0-2.6	4.5-5.5	8.0-13.5
MEAN	1799	105	294.5	293.9
ST. DEVIATION	617	55.3	2.33	2.38

TABLE VII. CORRELATION MATRIX, BLACK HILLS-2

CORRELATION	1.0-1.4	1.5-1.8	2.0-2.6	
1.0-1.4	1.000			
1.5-1.8	0.743	1.000		
2.0-2.6	0.518	0.908	1.000	
CHANNELS	1.0-1.4	1.5-1.8	2.0-2.6	
MEAN	1602	447	90.5	
ST. DEVIATION	463	154	38.7	

TABLE VIII. CORRELATION MATRIX, MONO LAKE

CORRELATION	1.0-1.4	2.0-2.6	4.5-5.5	
1.0-1.4	1.000			
2.0-2.6	0.892	1.000		
4.5-5.5	0.833	0.814	1.000	
CHANNELS	1.0-1.4	2.0-2.6	4.5-5.5	8.0-13.5
MEAN	2053	94.6	285.5	288.5
ST. DEVIATION	334	16.8	1.34	1.57

TABLE IX. CORRELATION MATRIX, PISGAH CRATER

CORRELATION	8.0-10.9	9.4-12.1	
8.0-10.9	1.000		
9.4-12.1	0.756	1.000	
CHANNELS	8.0-10.9	9.4-12.1	11.3-13.5
MEAN	288.2	288.0	288.7
ST. DEVIATION	2.38	2.47	2.88

TABLE X. DISTRIBUTION OF ELLIPSES BY AREA AT 1.5, 2.0, 2.5, and 3.0 σ THRESHOLDS FOR THE 9.3-11.7 μ m FLINT-1 IMAGE

SQUARE METERS			FREQUENCY			
			1.5 σ	2 σ	2.5 σ	3 σ
0.0	TO	10.0	256	244	100	22
10.0		15.0	165	143	50	9
15.0		20.0	156	118	42	4
20.0		25.0	104	86	29	3
25.0		30.0	85	55	16	0
30.0		40.0	154	103	13	4
40.0		50.0	154	72	10	1
50.0		60.0	92	31	7	2
60.0		70.0	61	12	1	1
70.0		80.0	29	5	1	1
80.0		90.0	17	3	1	1
90.0		100.0	5	2	1	0
100.0		150.0	13	7	2	1
150.0		200.0	7	1	2	1
200.0		500.0	4	4	4	1
500.0		1000.0	2	2	1	1
1000.0		2000.0	0	0	0	0
2000.0		5000.0	0	1	1	1
	Over	5000.0	1	0	0	0
TOTAL NUMBER OF						
TEMPERATURE THRESHOLDS =			1305	889	281	53

TABLE XI. DISTRIBUTION OF ELLIPSES BY AREA AT
 1.5, 2.0, 2.5, and 3.0 σ THRESHOLDS FOR
 THE 1.0-1.4 μ m FLINT-1 IMAGE

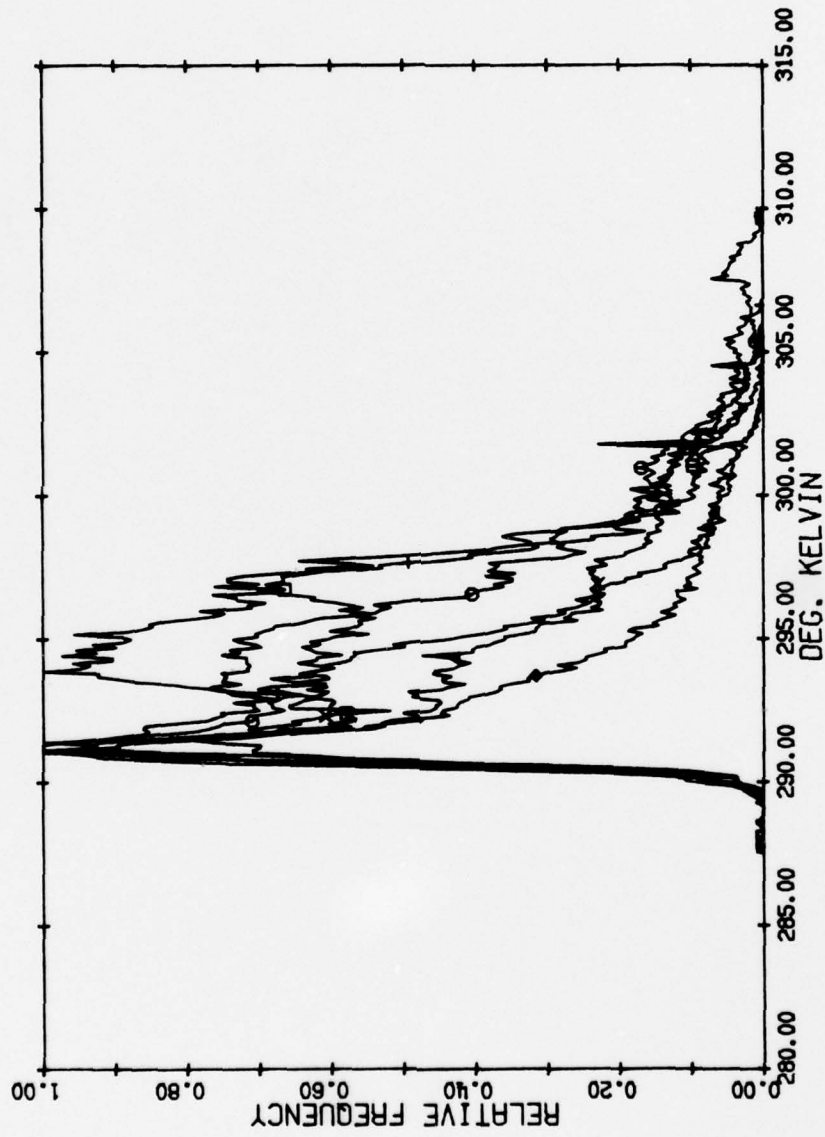
SQUARE METERS			FREQUENCY			
			1.5 σ	2 σ	2.5 σ	3 σ
0.0	TO	10.0	503	110	14	6
10.0		15.0	142	27	3	2
15.0		20.0	97	17	4	1
20.0		25.0	49	7	1	2
25.0		30.0	44	5	1	0
30.0		40.0	62	9	3	1
40.0		50.0	36	4	0	3
50.0		60.0	26	6	0	0
60.0		70.0	19	1	0	1
70.0		80.0	11	0	0	0
80.0		90.0	10	1	1	0
90.0		100.0	13	0	2	0
100.0		150.0	20	1	0	0
150.0		200.0	10	1	1	0
200.0		500.0	17	1	1	0
500.0		1000.0	4	0	1	1
1000.0		2000.0	0	1	0	0
2000.0		5000.0	1	0	0	0
	Over	5000.0	0	0	0	0
TOTAL NUMBER OF RADIANCE THRESHOLDS =			1064	191	32	17

TABLE XII. DISTRIBUTION OF ELLIPSES BY AREA AT
 1.5, 2.0, 2.5, and 3.0 σ THRESHOLDS FOR
 THE 9.3-11.7 μm WICHITA MOUNTAINS IMAGE

SQUARE METERS			FREQUENCY			
			1.5 σ	2 σ	2.5 σ	3 σ
0.0	TO	10.0	0	0	0	0
10.0		15.0	262	179	106	57
15.0		20.0	0	0	0	0
20.0		25.0	118	85	55	18
25.0		30.0	0	0	0	0
30.0		40.0	55	44	24	16
40.0		50.0	46	22	17	8
50.0		60.0	0	0	0	0
60.0		70.0	35	20	4	7
70.0		80.0	24	15	8	1
80.0		90.0	17	10	9	2
90.0		100.0	11	8	6	3
100.0		150.0	43	17	10	8
150.0		200.0	27	20	6	4
200.0		500.0	54	28	11	7
500.0		1000.0	21	10	2	1
1000.0		2000.0	11	5	5	0
2000.0		5000.0	5	6	2	1
	Over	5000.0	7	2	1	0
TOTAL NUMBER OF						
TEMPERATURE THRESHOLDS =			736	471	266	133

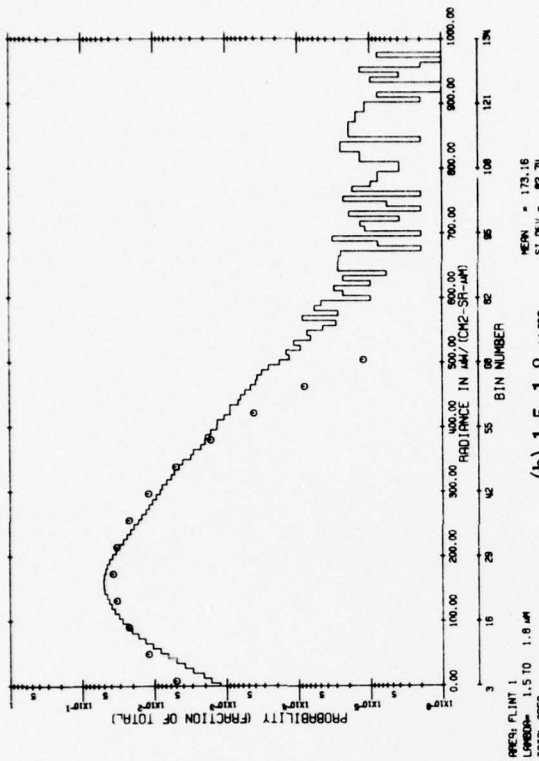
TABLE XIII. DISTRIBUTION OF ELLIPSES BY AREA AT
 1.5, 2.0, 2.5, and 3.0 σ THRESHOLDS FOR
 THE 1.0-1.4 μ m WICHITA MOUNTAINS IMAGE

SQUARE METERS			FREQUENCY			
			1.5 σ	2 σ	2.5 σ	3 σ
0.0	TO	10.0	0	0	0	0
10.0		15.0	90	54	53	107
15.0		20.0	0	0	0	0
20.0		25.0	47	36	32	32
25.0		30.0	0	0	0	0
30.0		40.0	30	20	14	14
40.0		50.0	19	15	12	12
50.0		60.0	0	0	0	0
60.0		70.0	15	11	8	5
70.0		80.0	16	14	9	0
80.0		90.0	5	11	4	2
90.0		100.0	10	4	6	1
100.0		150.0	27	9	14	6
150.0		200.0	18	11	7	1
200.0		500.0	25	26	15	7
500.0		1000.0	14	7	2	3
1000.0		2000.0	8	5	0	0
2000.0		5000.0	5	2	1	0
	Over	5000.0	8	4	3	0
TOTAL NUMBER OF						
RADIANCE THRESHOLDS =			337	229	180	190

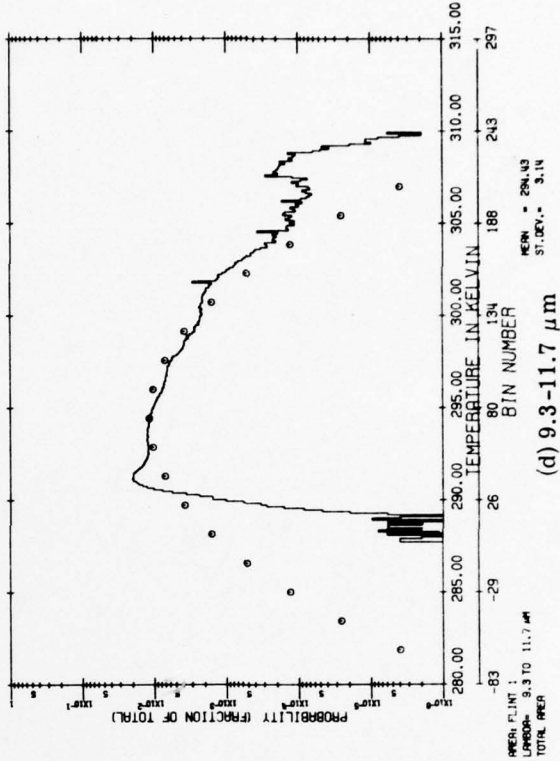


AREA: FLINT 1
 WAVELENGTH= 9.3 TO 11.7 μ M
 SUBRANGES

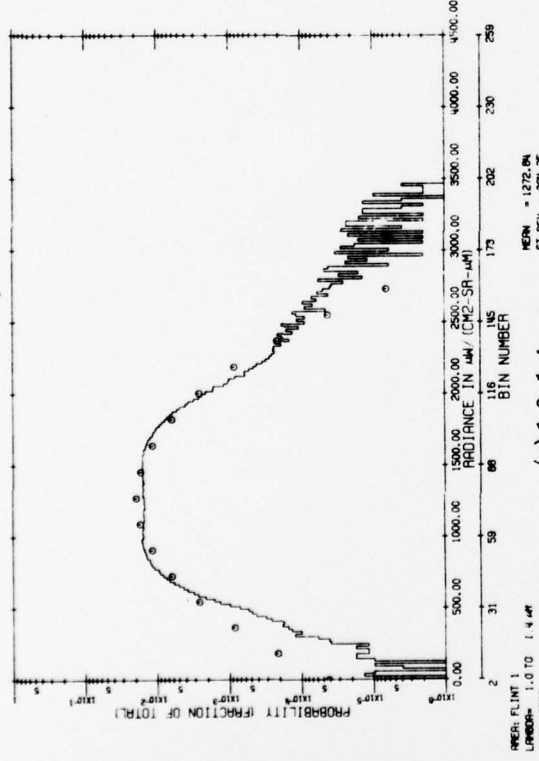
FIGURE 1. HISTOGRAM OF SIX AREAS WITHIN THE RESIDENTIAL FLINT-1 AREA
 IN THE 9.3-11.7 μ m SPECTRAL BAND



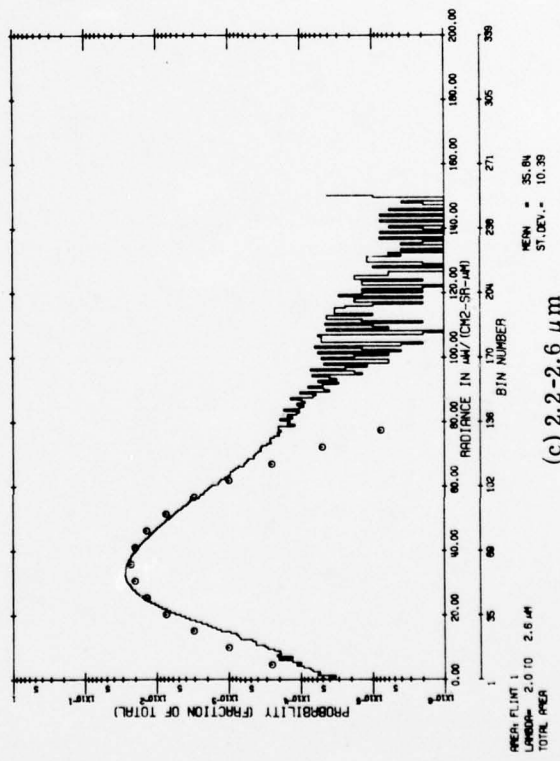
(a) 1.0-1.4 μm



(b) 1.5-1.8 μm

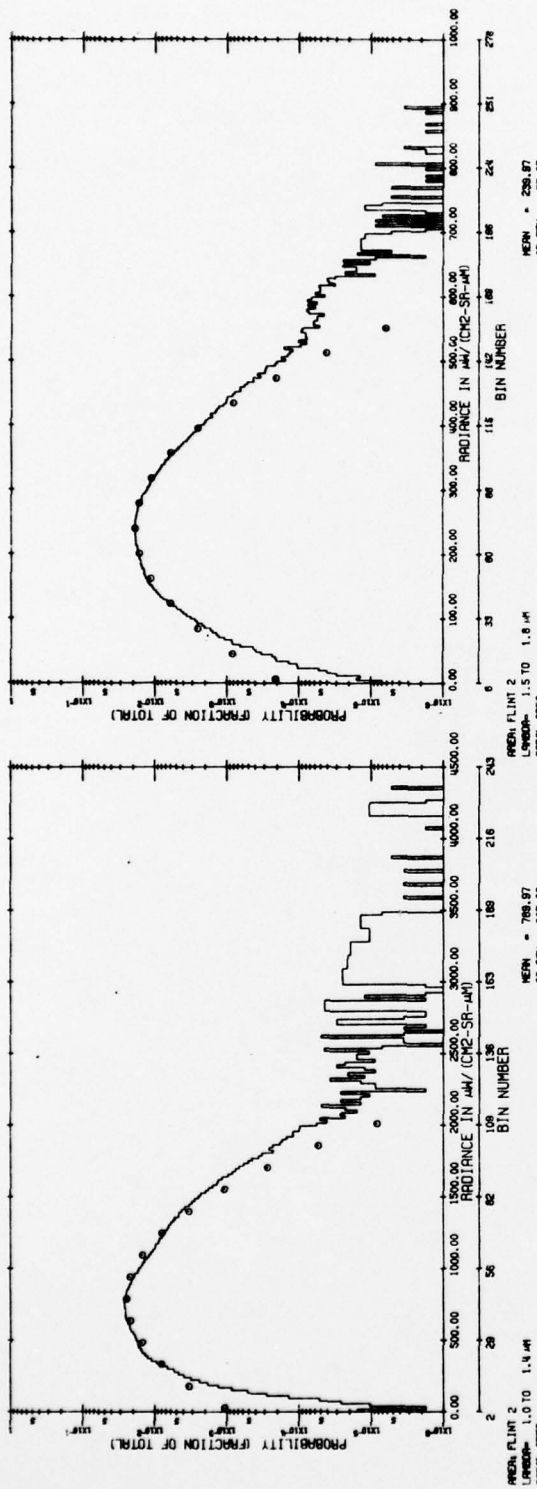


(c) 2.2-2.6 μm

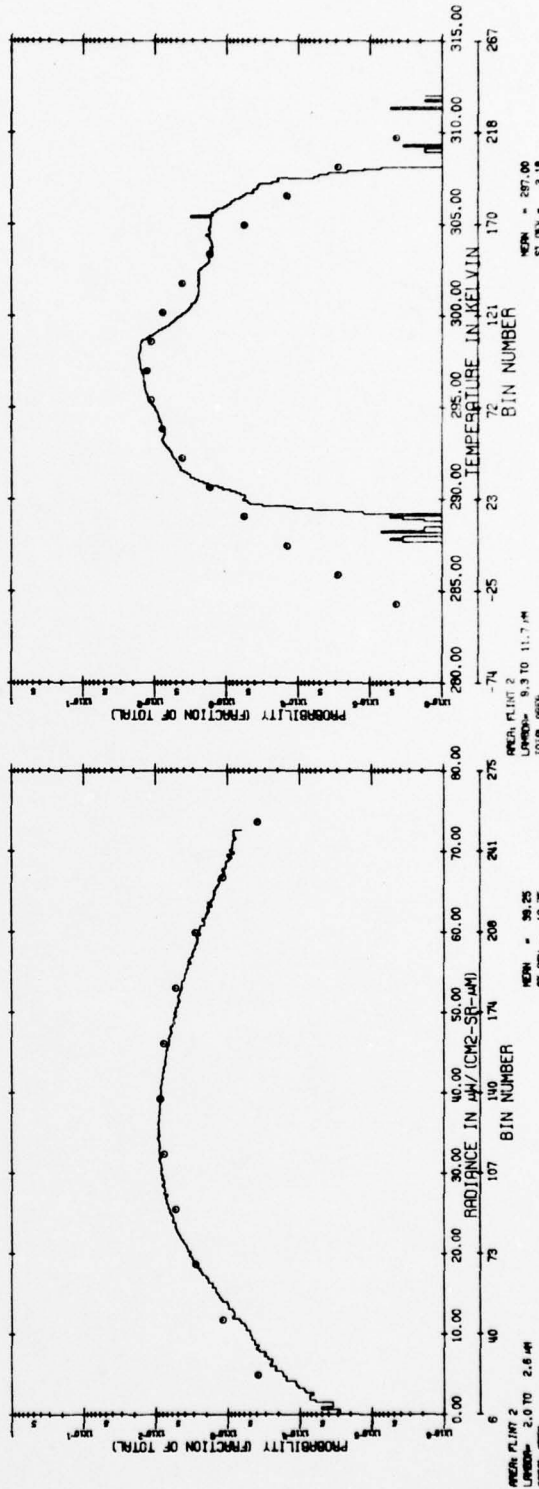


(d) 9.3-11.7 μm

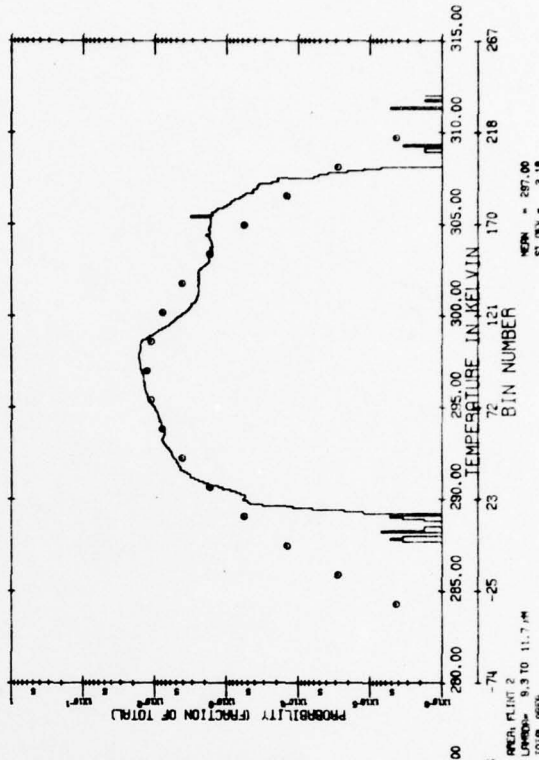
FIGURE 2. HISTOGRAM OF RESIDENTIAL FLINT-1 AREA



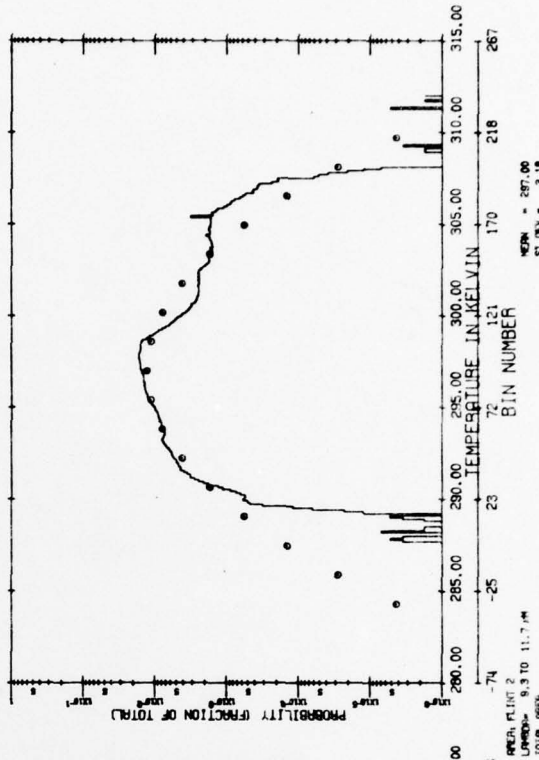
(a) 1.0-1.4 μm



(b) 1.5-1.8 μm

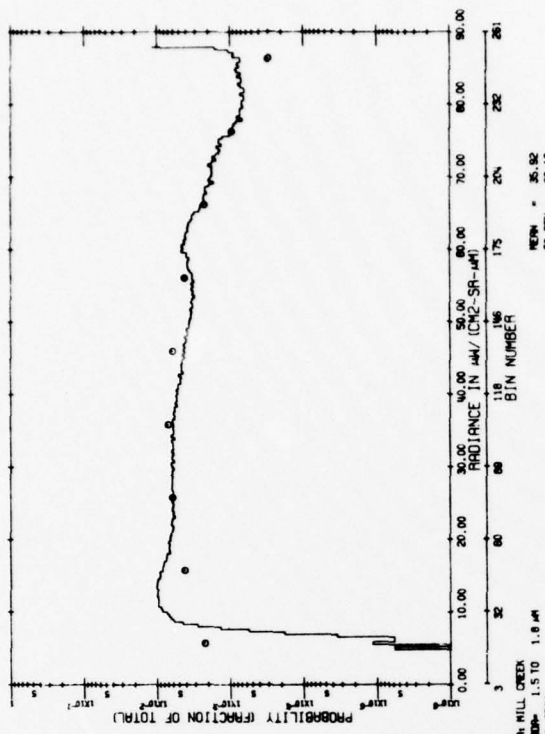


(c) 2.0-2.6 μm

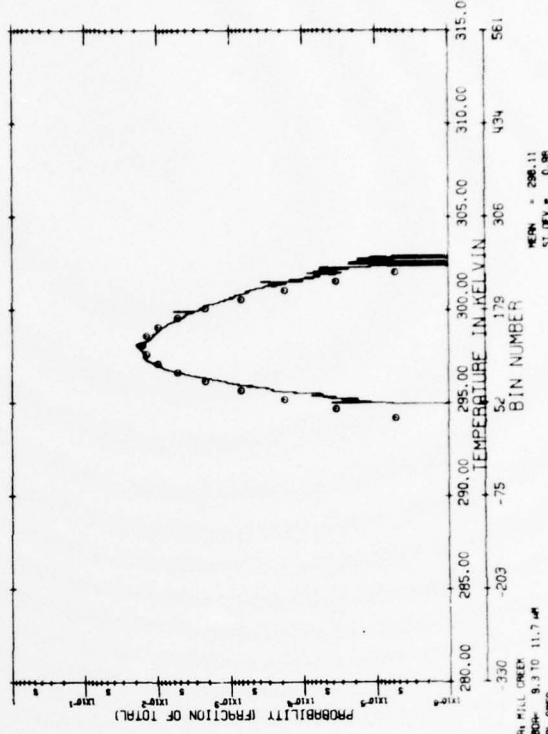


(d) 9.3-11.7 μm

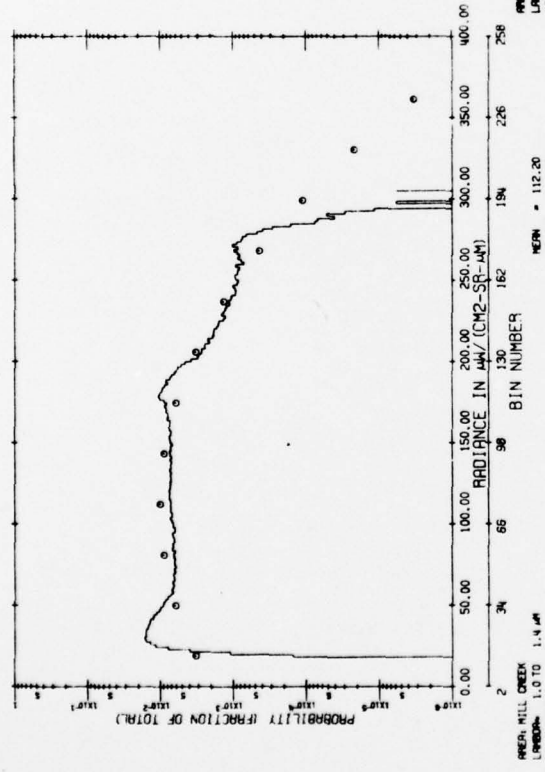
FIGURE 3. HISTOGRAM OF INDUSTRIAL FLINT -2 AREA



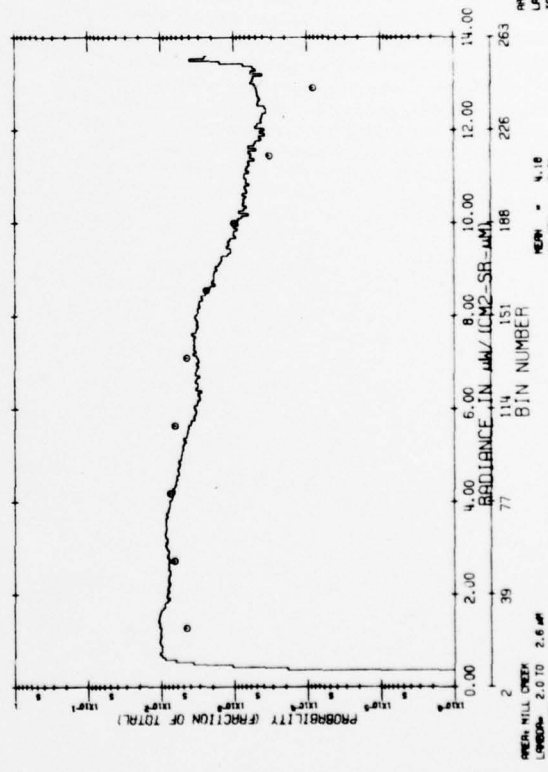
(a) 1.0-1.4 μm



(b) 1.5-1.8 μm

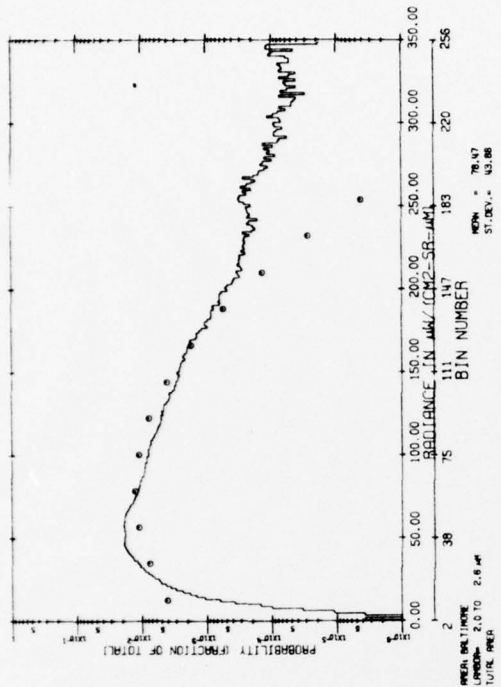


(c) 2.0-2.6 μm

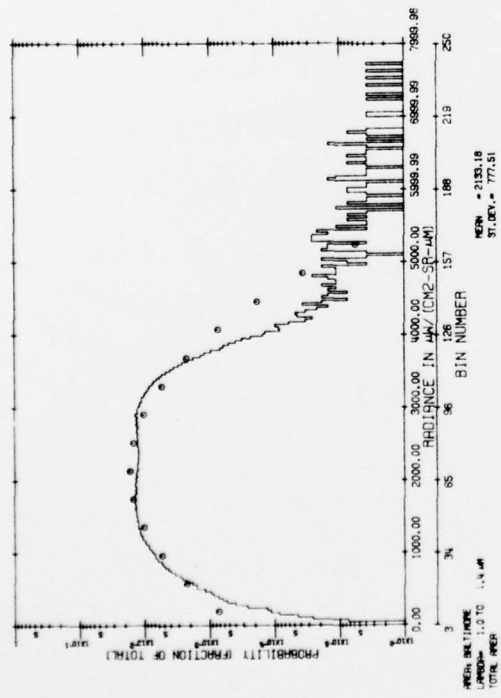


(d) 9.3-11.7 μm

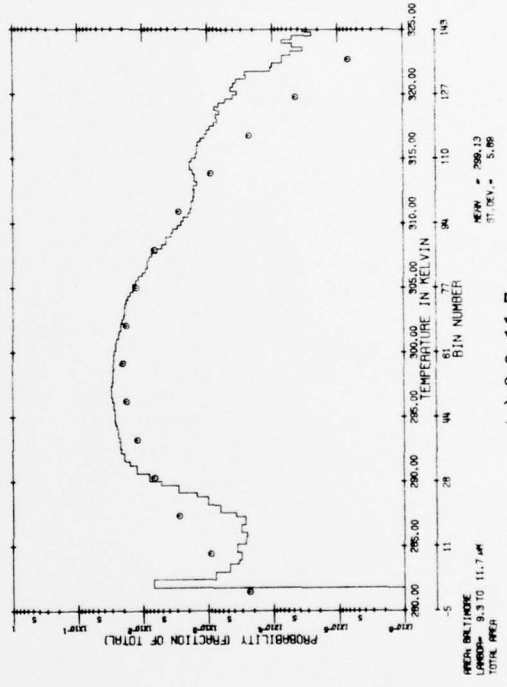
FIGURE 4. HISTOGRAM OF WICHITA MOUNTAINS, OKLAHOMA, MILL CREEK FLIGHT MISSION



(a) 1.0-1.4 μm

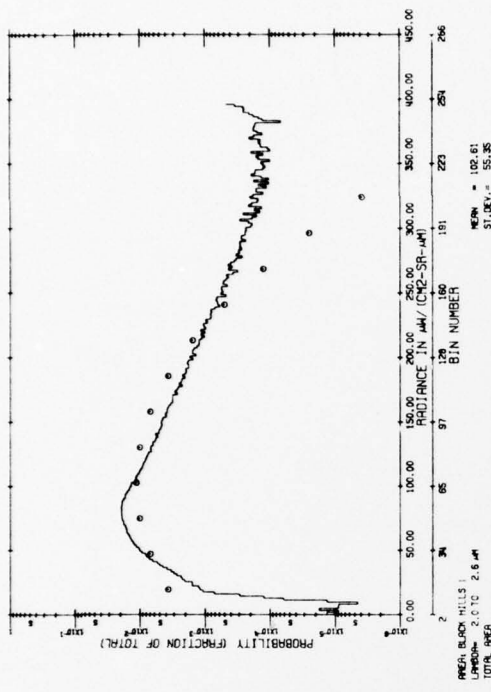


(b) 2.0-2.6 μm

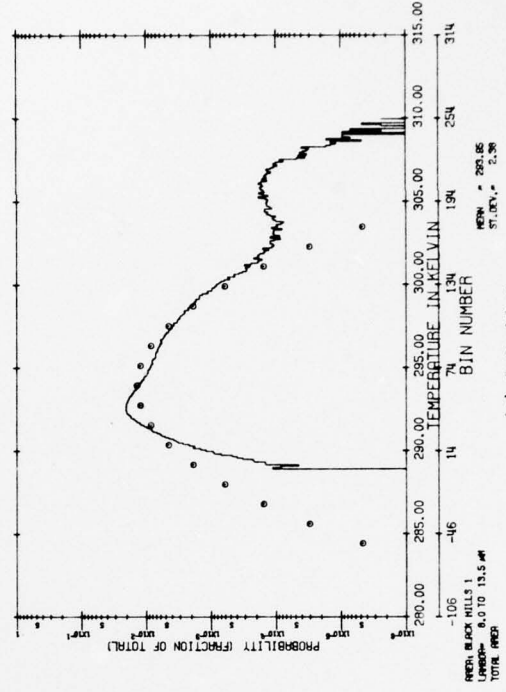


(c) 9.3-11.7 μm

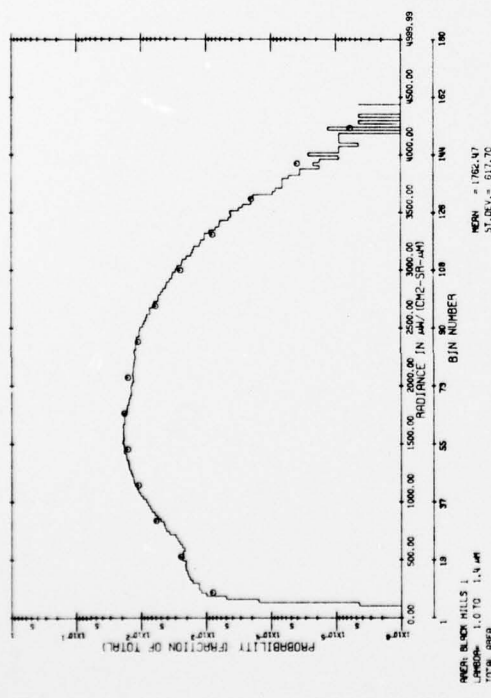
FIGURE 5. HISTOGRAM OF BALTIMORE AREA



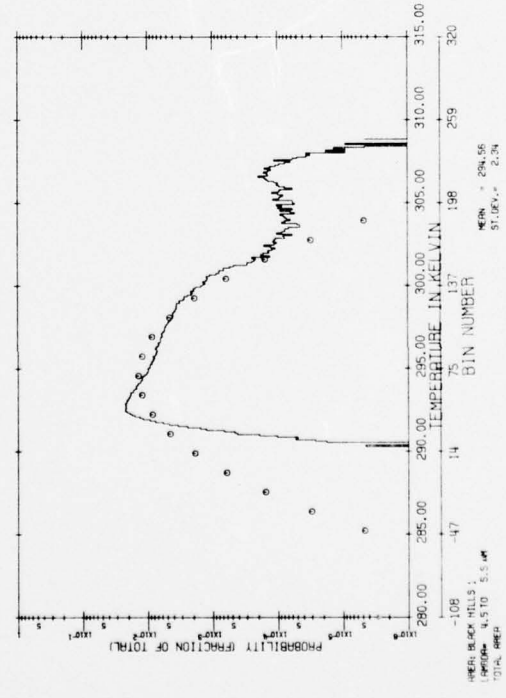
(b) 2.0-2.6 μ m



(d) 8.0-13.5 μ m

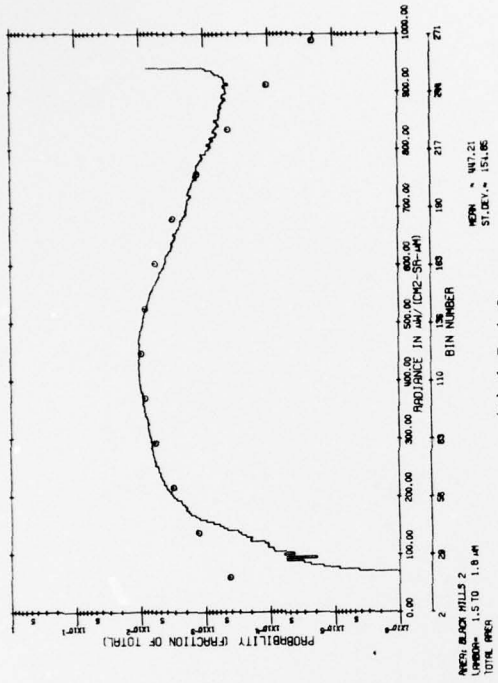


(a) 1.0-1.4 μ m

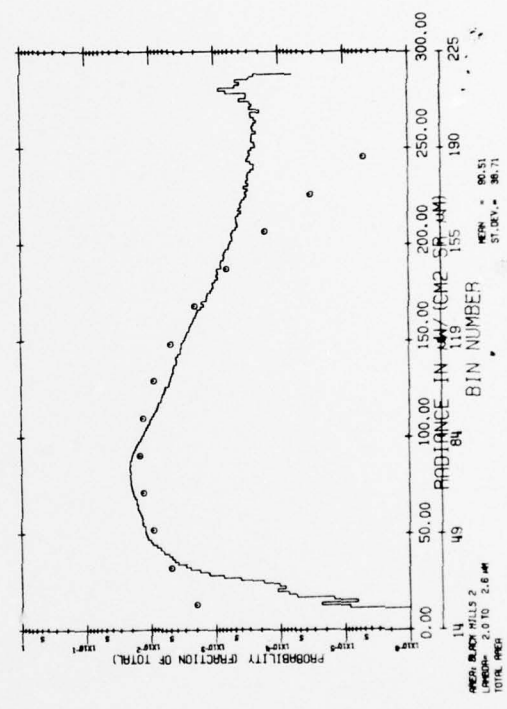


(c) 4.5-5.5 μ m

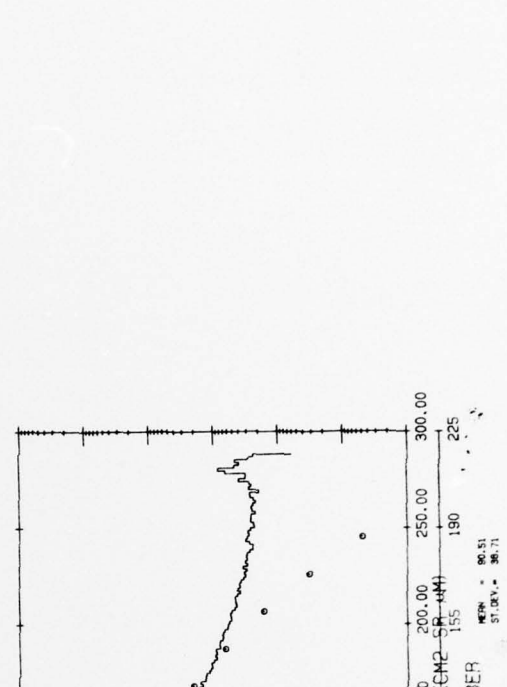
FIGURE 6. HISTOGRAM OF BLACK HILLS-1 AREA



(a) 1.0-1.4 μm

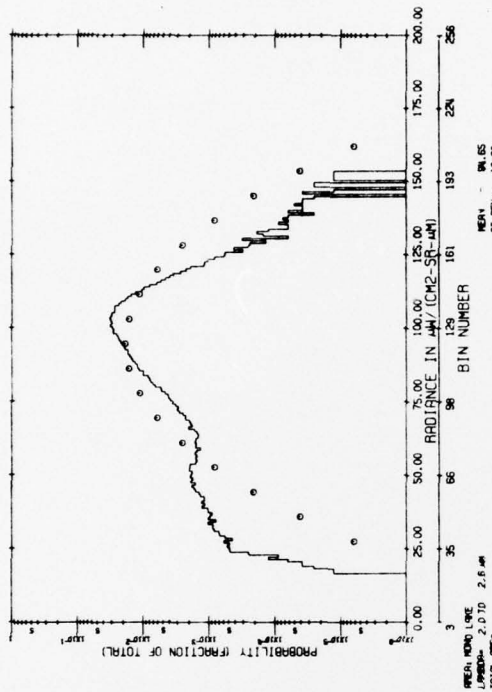


(b) 1.5-1.8 μm

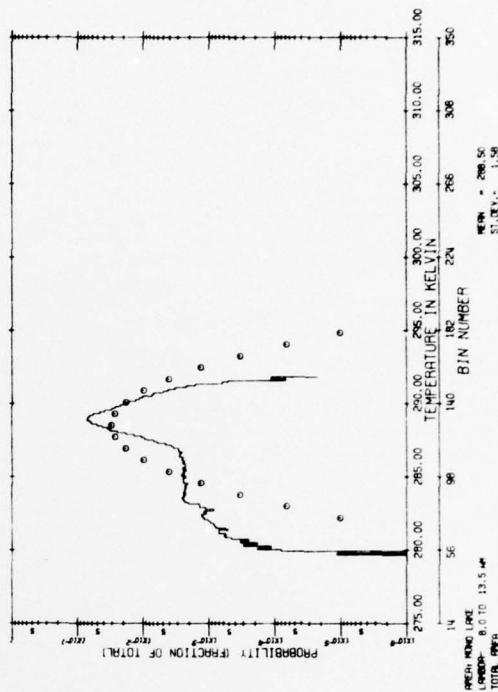


(c) 2.0-2.6 μm

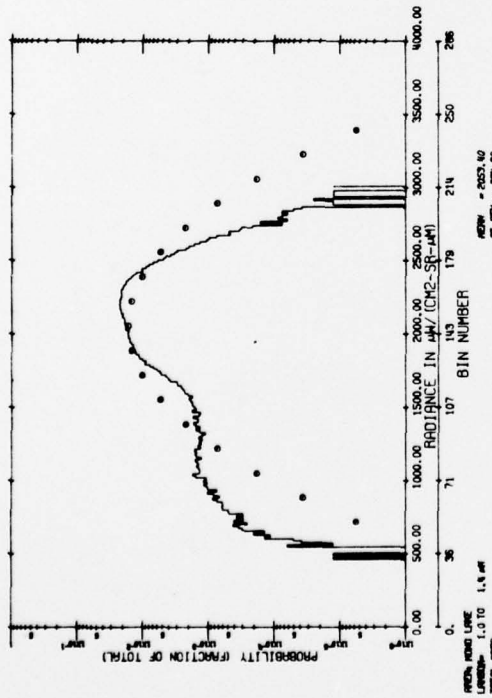
FIGURE 7. HISTOGRAM OF BLACK HILLS-2 AREA



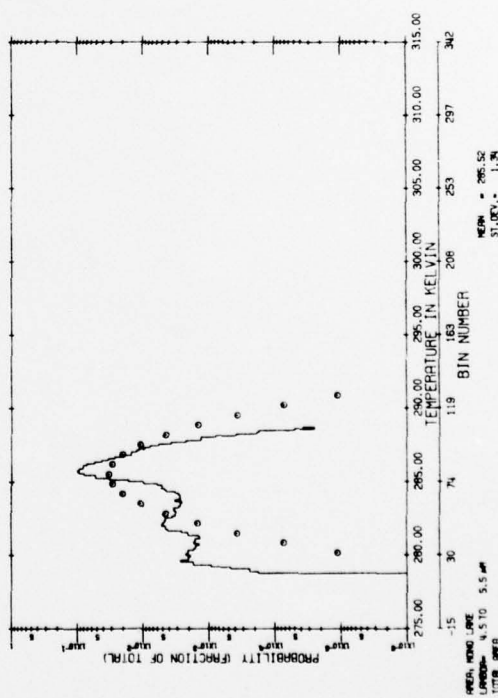
(a) 1.0-1.4 μm



(b) 2.0-2.6 μm

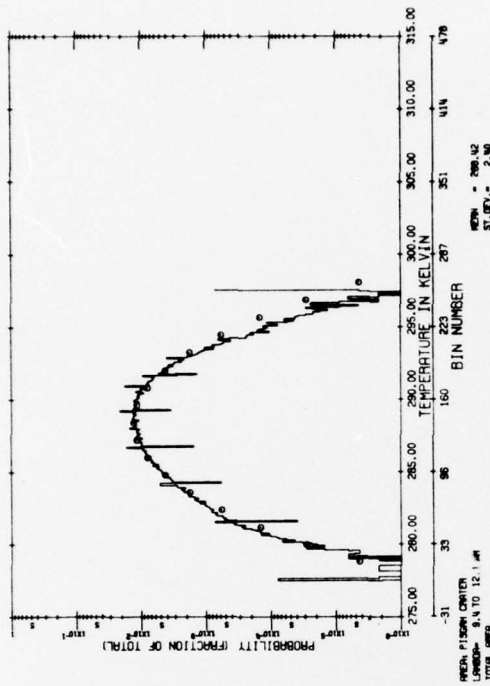


(c) 4.5-5.5 μm

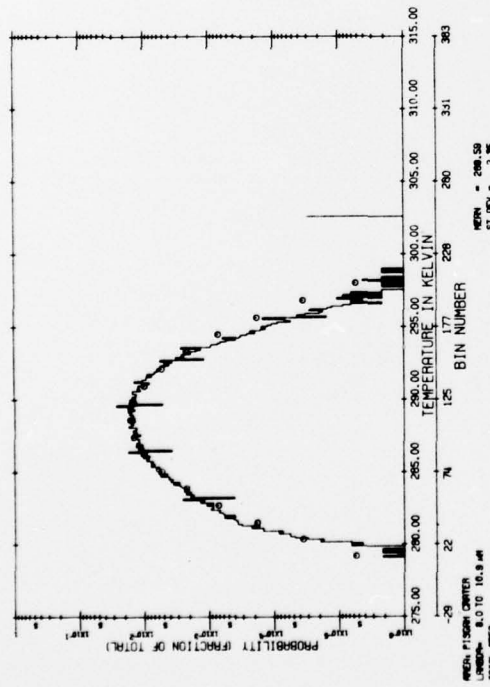


(d) 8.0-13.5 μm

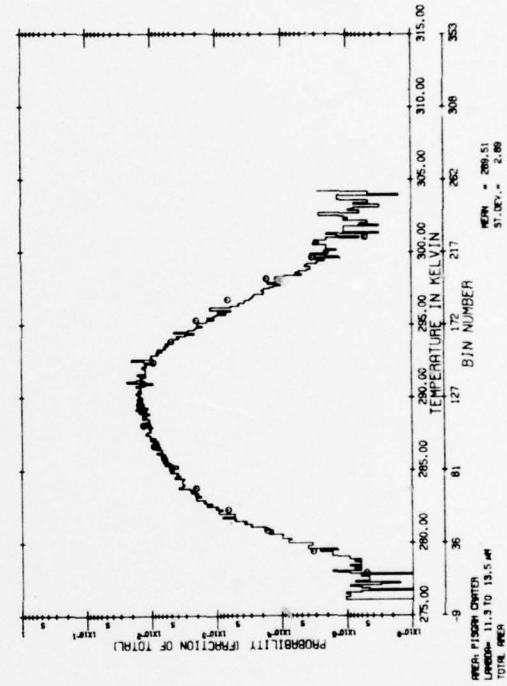
FIGURE 8. HISTOGRAM OF MONO LAKE AREA



(a) 9.4-12.1 μm

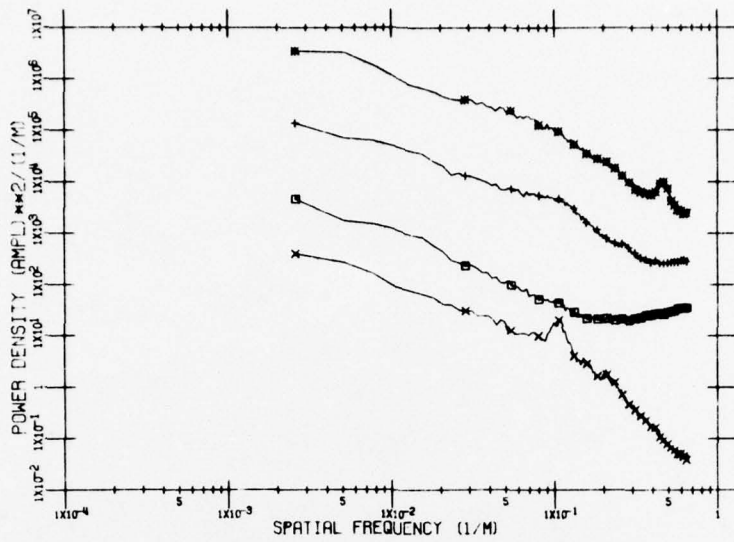


(b) 8.0-10.9 μm



(c) 11.3-13.5 μm

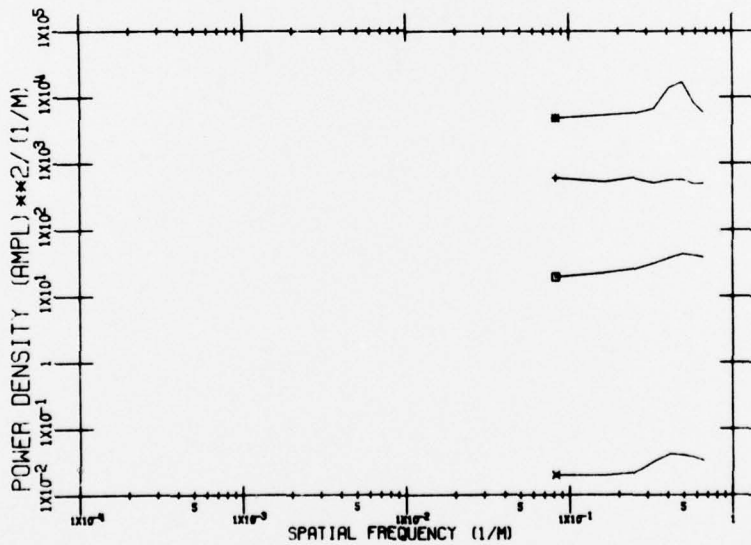
FIGURE 9. HISTOGRAM OF PISGAH CRATER AREA



AREA: FLINT 1
CROSSTRACK

LAMBDA = 1-1.4 (*), 1.5-1.8 (+), 2-2.6 (□), 9.3-11.7 (X) μm

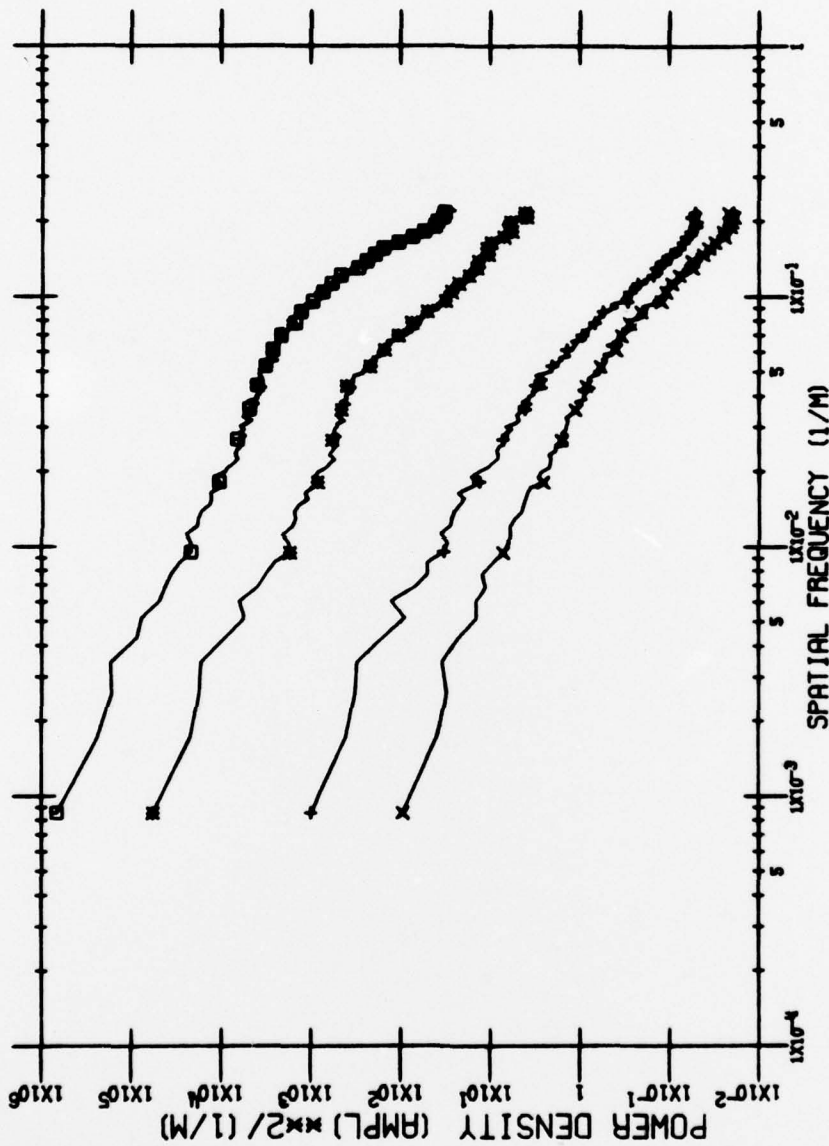
FIGURE 10. AVERAGE OF WIENER SPECTRUM OF EACH SCAN LINE IN FLINT-1 IMAGE. IN THE 1.0-1.4 μm BAND (*), IN THE 1.5-1.8 μm BAND (+), IN THE 2.0-2.6 μm BAND (□), AND IN THE 9.3-11.7 μm BAND (X).



AREA: FLINT 1
CROSSTRACK

LAMBDA = 1-1.4 (*), 1.5-1.8 (+), 2-2.6 (□), 9.3-11.7 (X) μm

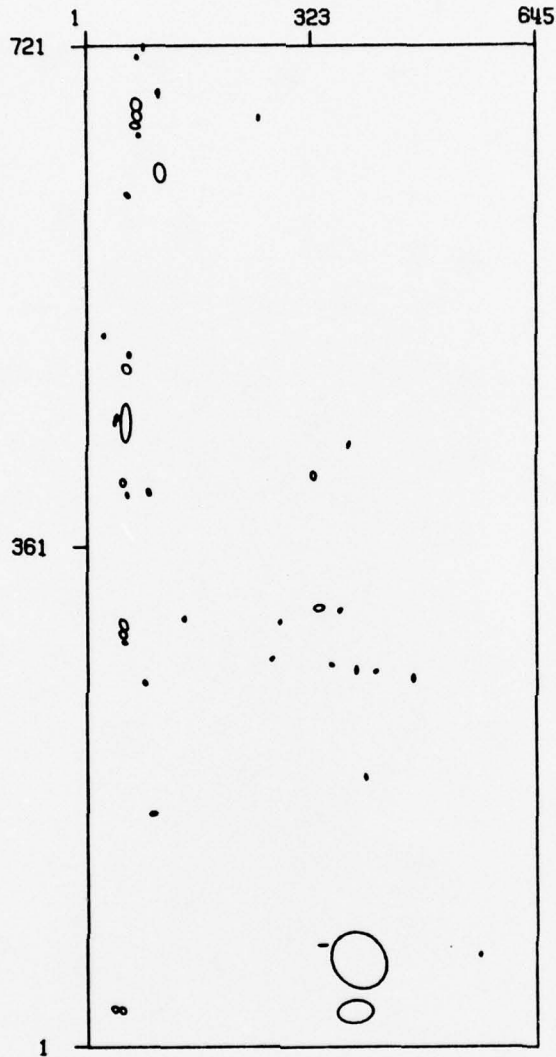
FIGURE 11. AVERAGE OF WIENER SPECTRUM OF A PORTION OF EACH SCAN LINE LOOKING AT UNIFORM DARK LEVEL WITHIN SCANNER HOUSING IN FLINT-1 IMAGE. IN THE 1.0-1.4 μm BAND (*), IN THE 1.5-1.8 μm BAND (+), IN THE 2.0-2.6 μm BAND (□), AND IN THE 9.3-11.7 μm BAND (X).



**AREA: MILL CREEK
CROSSTRACK**

LAMBDA = 1-1.4 (□), 1.5-1.8 (*), 2-2.6 (+), 9.3-11.7 (x) μm

FIGURE 12. AVERAGE OF WIENER SPECTRUM OF EACH SCAN LINE IN WICHITA MOUNTAINS, OKLAHOMA, DATA OF MILL CREEK MISSION. IN THE 1.0-1.4 μm BAND (□), IN THE 1.5-1.8 μm BAND (*), IN THE 2.0-2.6 μm BAND (+), AND IN THE 9.3-11.7 μm BAND (X).



FLINT 1

TEMPERATURE THRESHOLD = 3.00σ

LAMBDA= 9.3 TO 11.7 μM

FIGURE 13. EQUIVALENT ELLIPTICAL AREAS FOR CONTIGUOUS AREA IN THE FLINT-1 IMAGE WITH APPARENT TEMPERATURES GREATER THAN 303.8 K OR 3σ ABOVE THE MEAN.

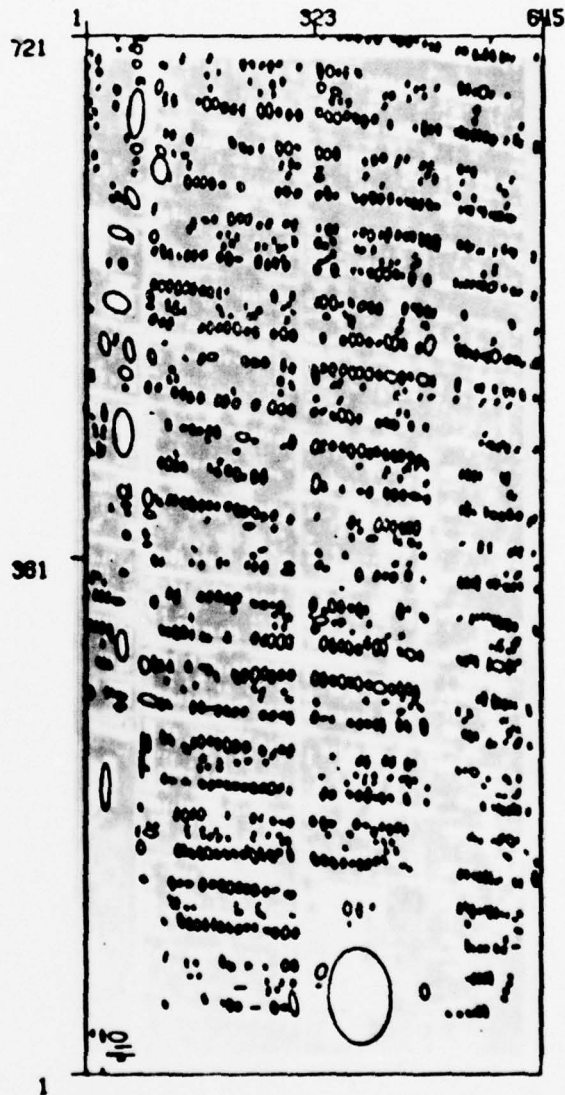
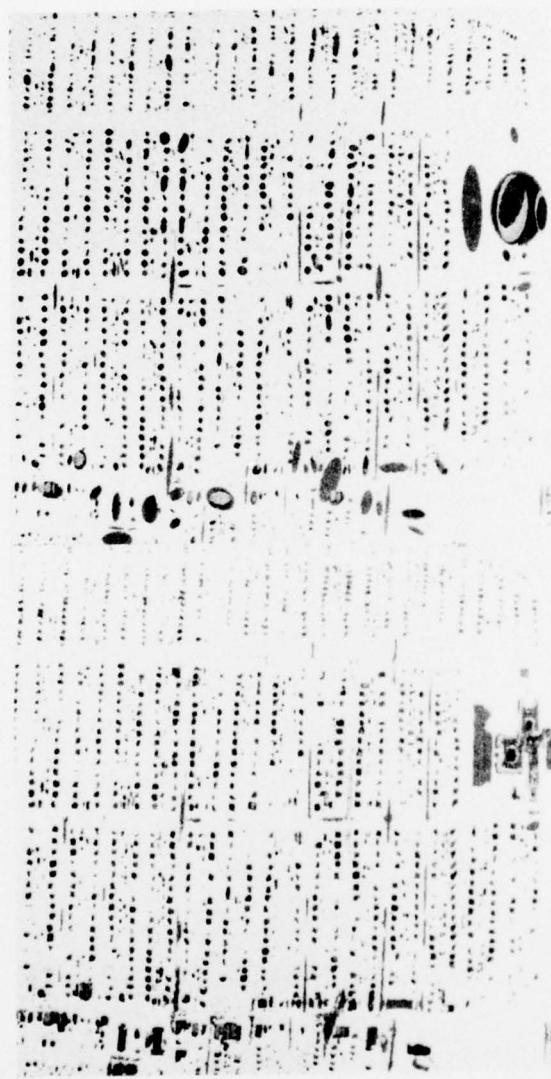


FIGURE 14. EQUIVALENT ELLIPTICAL AREAS FOR CONTIGUOUS AREAS IN THE FLINT-1 IMAGE WITH APPARENT TEMPERATURE GREATER THAN 299.1 K OR 1.5σ ABOVE THE MEAN SUPERIMPOSED ON THE ACTUAL FLINT-1 9.3-11.7 μm IR IMAGE



Blue = 296-301°K
 Green = 301-304°K
 Brown = <293°K

ARTIFICIAL COLOR IMAGE OF THE
 9.3-11.7 μm CHANNEL OF FLINT-1.

Yellow = 304-307°K
 Red = 307-310°K

ARTIFICIAL COLOR REPRESENTATION OF THE
 PSEUDO-IMAGE GENERATED FROM THE
 9.3-11.7 μm CHANNEL OF FLINT-1.

FIGURE 15. ACTUAL IMAGE OF FLINT-1 (LEFT) AND AN ELLIPSE REPRESENTATION OF FLINT-1 IMAGE (RIGHT).

REFERENCES

- [1] J. Beard, J. Braithwaite, R. Turner, Infrared Background Survey and Analysis, Report 118000-1-F, Environmental Research Institute of Michigan, Ann Arbor, June 1976.
- [2] Philip G. Hasell, Jr., et al, Collation of Earth Resources Data Collected by ERIM Airborne Sensors, Report 109600-33-F, Environmental Research Institute of Michigan, Ann Arbor, September 1975.
- [3] R. Spellicy, J. Beard, J. R. Maxwell, Statistical Analysis of Terrain Background Measurements Data, Report No. 120500-12-F, Environmental Research Institute of Michigan, Ann Arbor, March 1977.